IEEE Access
Multidisciplinary ⋮ Rapid Review ⋮ Open Access Journal

Received January 27, 2022, accepted February 15, 2022, date of publication February 22, 2022, date of current version March 29, 2022.

Digital Object Identifier 10.1109/ACCESS.2022.3153096

Concentric Annular Leaky Wave Antenna Array and Its Application to Self-Sensing Smart Antenna for Radio Wave Coverage in 2-D Confined Spaces

YUCHEN MA[1], JUNHONG WANG[2], (Senior Member, IEEE), CHONG PAN[1], YING ZHU[1], AND XIANG WU[1]

[1]China Academy of Information and Communications Technology, Beijing 100191, China
[2]Key Laboratory of all Optical Network and Advanced Telecommunication Network, Ministry of Education of China, Beijing Jiaotong University, Beijing 100044, China

Corresponding author: Junhong Wang (wangjunh@bjtu.edu.cn)

This work was supported in part by the National Natural Science Foundation of China (NSFC) Project under Grant 62031004 and Grant 61871025.

ABSTRACT A beam-changeable concentric annular Leaky-Wave Antenna (LWA) array is proposed, which contains two annular LWAs with constant-interval slots. By changing the excitations of the two LWAs, the radiation beam can be changed to different shapes and in different directions i.e. single beam to normal direction, conical beam to 40° and a synthetic beam. A theoretical model for analyzing the radiation properties of the LWA array is put forward, and a prototype of the array with the radius of 42.6 mm and the height of 4 mm is fabricated. By comparing simulation and the measurement results, it is found that the proposed LWA array exhibits a very well expected performance. The proposed antenna array is then applied to construct a self-sensing smart antenna which can provide flexible radio wave coverage according to the positions of users. Image-aware function is integrated into the smart antenna, and a series of tests including received power and Error Vector Magnitude (EVM) measurements are carried out in indoor scenarios. The results verify the effectiveness of the design.

INDEX TERMS Leaky wave antenna array, theoretical model, pattern synthesis, beamforming, smart antenna.

I. INTRODUCTION

For the next generation of mobile communication, multi-beam and beam-changeable antennas will provide flexible radio wave coverage and ensure the quality of mobile communication, which are attracting increasing attention. Many works about multi-beam and beam-changeable antennas have been published. In [1], a wideband Circularly Polarized (CP) end-fire multi-beam antenna array is proposed. In [2], a Rotman lens-fed low sidelobe multi-beam array antenna is designed. In [3], an array antenna fed by 4 × 4 Butler matrix is presented to provide two-dimensional multi-beam. In [4], a planar holographic leaky-wave antenna capable of generating four beams simultaneously is designed. In [5], a 3-D printed wideband Cassegrain antenna for linear multi-beam is proposed. By stacking five Cassegrain sub-arrays with different tilt angles, 2-D multi-beam radiation can be realized. In [6], by using a lens cavity with seven input ports, a fourteen-element array antenna with multi-beam property is achieved. In [7], a broadband CP multi-beam antenna with an anisotropic impedance surface superstrate is proposed, which generates five pencil beams covering a range of (−33°, +33°). In [8], a beam-steering gravitational Liquid antenna is proposed, of which the beam is stable upward regardless of the antenna postures. In addition, beam-changeable antennas are capable of changing their beams in different shapes and to different directions, and providing radio wave coverage over different desired regions. In [9], a direction-changeable concentric conical beam array antenna achieved by superimposing different conical beams is proposed. In [10], a pattern-synthesis method based on characteristic mode analysis is proposed, by which antenna patterns with null in the axial direction and omni-directional in the perpendicular plane can be obtained. In [11], a unidirectional loop antenna that can achieve pattern reconfiguration from −40° to +40° in the azimuth plane is presented, where

The associate editor coordinating the review of this manuscript and approving it for publication was Kai-Da Xu.

the loop is loaded with p-i-n diodes and the radiation pattern can be rotated by controlling the diodes states. In [12], a beam changeable Fabry–Pérot antenna using a liquid-metal partially reflective surface is proposed. By injecting the liquid metal into the microfluidic channels under specifically designed elements, the beam direction and beamwidth can be changed. In [13], a graphene-based pattern-reconfigurable antenna controlled by voltage to generate two beams is designed. In [14], a beam changeable 4 × 4 antenna array based on digital coding method is proposed. In [15], by using a reconfigurable feeding structure, a pattern-reconfigurable high gain spherical dielectric resonator antenna operating on TE_{301} mode is proposed. Although these antennas are capable of changing their beams, to further improve the communication quality, smart antennas with automatic beam-changing are preferable. In [16], a smart antenna with automatic beam switching based on Frequency Modulated Continuous Wave (FMCW) is proposed, which is designed for one-dimensional radio wave coverage. In [17], an image-aware smart antenna providing beam tracking is designed for two-dimensional scenarios. These two antennas have the function of automatic beam-changing according to the positions of users in real time.

In this paper, a beam-changeable concentric annular LWA array is proposed. Comparing to the multi-beam antennas in [1]–[8], [16], [17] which mostly provides only directive switchable beams, this work generates multi-beams including directive beam, omnidirectional beam and synthetic beam. This adapts to more coverage demands. Furthermore, although the beam-changeable antennas in [9]–[15] reconfigures their beams to different shapes, the hand over should be controlled and excited by the remote processing center. Instead, the array in this paper enables its beams to adaptively change both in direction and beamwidth aligning with the changing of the environment and targets, which empowers the antenna itself with the perceiving and processing abilities. In this paper, a theoretical model to analyze the radiation property of the array is presented in Section II. The experimental validation of the proposed LWA array is implemented in Section III. In Section IV, a self-sensing smart antenna is constructed by integrating the proposed LWA array with an image-aware circuit, and its performance is verified in a real indoor scenario. Conclusion is drawn in Section V.

II. MODELLING AND ANALYSIS

In this section, a theoretical model of the two-annular LWA array is given first. Then, in terms of radiation property, a series of variable analysis is implemented based on the theoretical model.

A. THEORATICAL MODEL OF ANNULAR ARRAY

In the previous work, theoretical model for single annularly slotted LWA is proposed [18], by which the radiation properties can be investigated and analyzed, and conical beam with desired conical angle can be designed. Here, the model

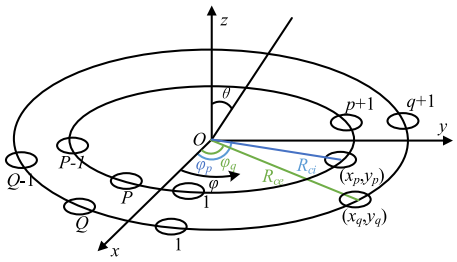

FIGURE 1. Spatial model of concentric slotted annular array excited by traveling-wave.

is extended to the concentric LWA array, as shown in Fig. 1. The array is composed of two annular LWAs. The numbers of units contained in the inner and outer LWAs are denoted by P and Q respectively. Due to the property of travelling wave, each unit has a phase delay along the wave propagation direction. Here, we assume that the direction of travelling wave in the array is anticlockwise. It is noted that, although the array is designed for multi-beam mode working, when exciting its elements individually, the two-looped LWA array is simplified to two single annular LWAs, whose radiation property have been analyzed in [18].

When exciting the two-annular LWAs simultaneously, the far field of the array is expressed by

$$\begin{aligned} \mathrm{E}_\theta(\theta,\varphi) = &\sum_{p=1}^{P} a_p E_{\theta s}(\theta, \varphi-(p-1)\theta_{si}-\theta_{bi}) e^{-\mathrm{j}\phi_p} \\ &+ \sum_{q=1}^{Q} a_q E_{\theta s}(\theta, \varphi-(q-1)\theta_{se}-\theta_{be}) e^{-\mathrm{j}\phi_q} e^{-\mathrm{j}\delta\phi} \end{aligned} \tag{1}$$

$$\begin{aligned} \mathrm{E}_\varphi(\theta,\varphi) = &\sum_{p=1}^{P} a_p E_{\varphi s}(\theta, \varphi-(p-1)\theta_{si}-\theta_{bi}) e^{-\mathrm{j}\phi_p} \\ &+ \sum_{q=1}^{Q} a_q E_{\varphi s}(\theta, \varphi-(q-1)\theta_{se}-\theta_{be}) e^{-\mathrm{j}\phi_q} e^{-\mathrm{j}\delta\phi} \end{aligned} \tag{2}$$

where $E_{\theta s}$ and $E_{\varphi s}$ are the far field components of a unit, which are calculated by electric field integration method introduced in [18]. a_p and a_q are the radiating field amplitudes of slots of the inner and outer LWAs respectively, which are calculated by

$$\alpha = -\ln(|S_{21}|/\sqrt{1-|S_{11}|^2})/L \tag{3}$$

where L is the length of the LWAs. It is worth noting that when two-annular LWAs are excited at the same time, mutual coupling will occur. The calculation of a_p and a_q needs to consider the coupling between the LWAs. However, if the isolation of the two LWAs is large enough, the effect of mutual coupling can be ignored and a_p and a_q can be gotten by the formula for the two single LWAs. θ_{si} and θ_{se} are the angular intervals of the two LWAs, and θ_{bi} and θ_{be} are

the initial angles of the first slots counted from x-axis for the inner and outer LWAs respectively. $\delta\phi$ is the difference between the initial feeding phases of the inner and outer LWAs. The initial feeding phases of slots in the array is expressed by

$$\begin{cases} \phi_p = (p-1) \times \frac{2n_1\pi}{P}, & p = 1, 2, \ldots, P \\ \phi_q = (q-1) \times \frac{2n_2\pi}{Q}, & q = 1, 2, \ldots, Q \end{cases} \tag{4}$$

where $2n_1\pi$ and $2n_2\pi$ is the total phase variation in the inner and outer LWAs respectively.

Hence, by using the two-annular LWA theoretical model, far field of the concentric LWA array can be predicted.

B. ANALYSIS OF RADIATION PROPERTIES

In order to analyze the array by theoretical model, aperture field of one slot in the concentric LWA array is extracted. By adjusting the widths of the waveguides according to the radiation condition in [19], fundamental wave of TE_{10} mode is allowed to exist only. The radii of the two LWAs are set to $R_{ci} = 11.3$ mm and $R_{ce} = 32.5$ mm. The operating frequency is 5.8 GHz. The effect of wavelength numbers of the inner and outer LWAs, n_1 and n_2, which are the two important parameters, on the radiation properties is studied first. The initial feeding phases of the two LWAs are assumed to be zero, and $\delta n = n_2 - n_1$. In addition, the aperture field amplitudes of all slots in one LWA are assumed to be the same, and the wave in the two LWAs has the same travelling direction (anticlockwise). When $\delta n = 0$, the total phase variations in the inner and outer waveguides are the same. In this case, it is expected that the proposed concentric LWA array has a higher gain than a single annular LWA. When $n_1 = n_2 = 1$, a broadside beam is generated. If $n_1 = n_2 > 1$, conical beam with increasing conical angle is generated, as illustrated in Fig. 2(a). On the other hand, for the situation of $\delta n \neq 0$, canceling of radiation field will occur in some azimuth direction, and the lobe number n_{lobe} is related to δn, which is expressed by

$$n_{lobe} = \delta_n \tag{5}$$

In this case, the radiation pattern is not omnidirectional in azimuth plane. The radiation pattern in Fig. 3 is the circumferential pattern when θ equals to the angle of maximum radiation direction. When $\delta n = 1$, the main beam is unidirectional and located in yoz-plane, which can be seen from Fig. 2(b) and Fig. 3(a). The consequence can be explained by the leaky-wave antenna theory. It is well known that fundamental wave of TE_{10} mode on traveling wave antenna produces forward radiation. So for the two traveling wave excitation sources with the same initial phase and the anticlockwise direction, the far field generated by the two rows of slots near the $+x$ axis will be superimposed in $+y$ axial direction, and no radiation will be generated in -y axial direction. The radiation generated by the two rows of slots near the -x axis should be in the -y axial direction. However, as $\delta n = 1$, the excitations of the inner and outer

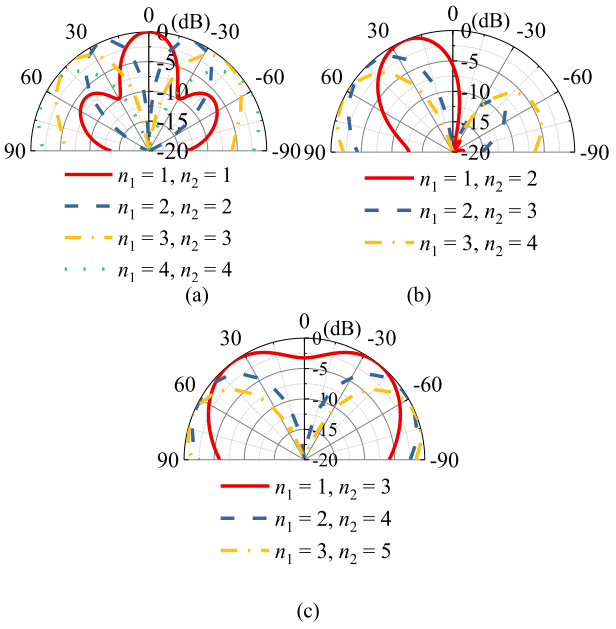

FIGURE 2. Radiation patterns of the concentric LWA array with different δn in *yoz* -plane given by the theoretical model, (a) $\delta n = 0$, (b) $\delta n = 1$, (c) $\delta n = 2$.

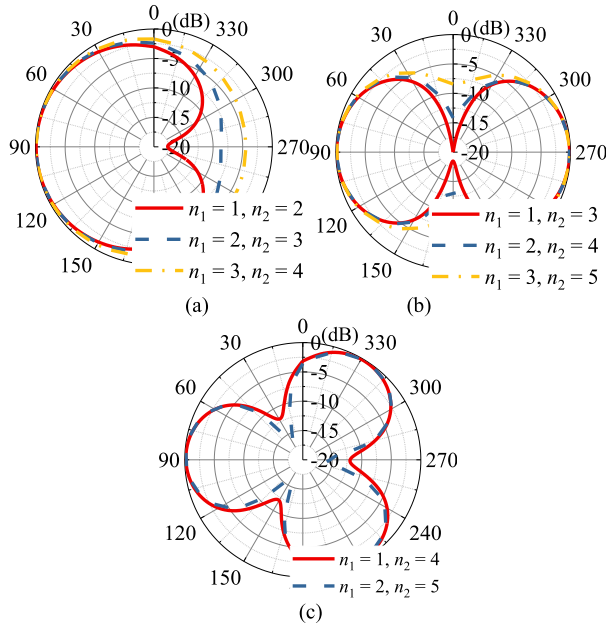

FIGURE 3. Radiation patterns of the concentric LWA array in the conical plane when θ equals to the maximum radiation angle, with different δn given by the theoretical model, (a) $\delta n = 1, \theta = 24°, 47°, 64°$, (b) $\delta n = 2, \theta = 38°, 60°, 71°$, (c) $\delta n = 3, \theta = 45°, 65°$.

slots are out of phase, so the far fields of the two rows of slots cancel each other in the -y axial direction, and hence there is no radiation in the $+y$ and -y axial directions. The phase difference between the inner and outer slots at other positions is between 0 and π, so the radiation of them cannot be completely superimposed or cancelled, and a field between the above two extreme cases is obtained. Therefore, for the whole array, the main radiation direction is in the $+y$ axial direction, that is, in the plane of $\varphi = 90°$. When

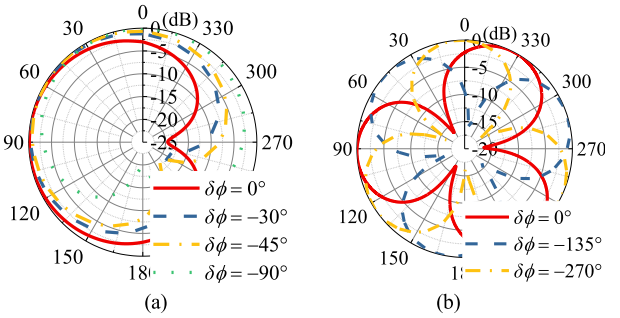

FIGURE 4. Radiation patterns of the concentric array for different $\delta\phi$ in azimuth plane predicted by the theoretical model, (a) $n_1 = 1, n_2 = 2, \theta = 24°$, (b) $n_1 = 1, n_2 = 4, \theta = 45°$.

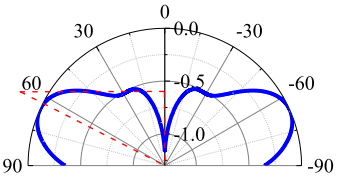

FIGURE 5. Calculated radiation pattern of cosecant-squared distribution of the concentric array, the normalized amplitudes of the inner and outer LWAs are 1 and 0.25, R_{ci} and R_{ce} are set to 11.3 mm and 29 mm, $n_1 = n_2 = 2$.

$\delta n = 2$, there are bilateral beams in *yoz*-plane, as illustrated in Fig. 2(c), and Fig 3(b). For $\delta n = 3$, there are three beams with interval of 120° in azimuth plane, as illustrated in Fig. 3(c).

Furthermore, the initial phases of the two LWAs are also crucial to radiation patterns. By changing $\delta\phi$, the radiation pattern of the array can be arbitrarily rotated around the array center. The relationship between the rotating angle θ_r and $\delta\phi$ is expressed as

$$\theta_r = -\delta\phi / \delta_n \tag{6}$$

Fig. 4 (a) and (b) show the radiation patterns in azimuth plane for different $\delta\phi$, when $\delta n = 1$and3 respectively. It can be observed from the figures that the proposed model predicts the radiation patterns well.

In particular, as we know, for uniform radio wave distribution, beamforming antennas generating cosecant-squared beams are attractive and useful [20]. Here, based on the proposed concentric LWA array, two-dimensional cosecant-squared beam is obtained by adjusting the radius and excitation amplitudes of the two LWAs. The radiation pattern in *xoz*-plane is shown in Fig. 5.

III. EXPERIMENTAL VALIDATION

In order to validate the proposed method, a concentric LWA array was fabricated. Measurement was carried out by Agilent E8363C PNA network analyzer in an anechoic chamber.

A. STRUCTURE DESIGN AND FABRICATION

As known, Substrate-Integrated Waveguide (SIW) is commonly used for low profile antennas, especially in the design

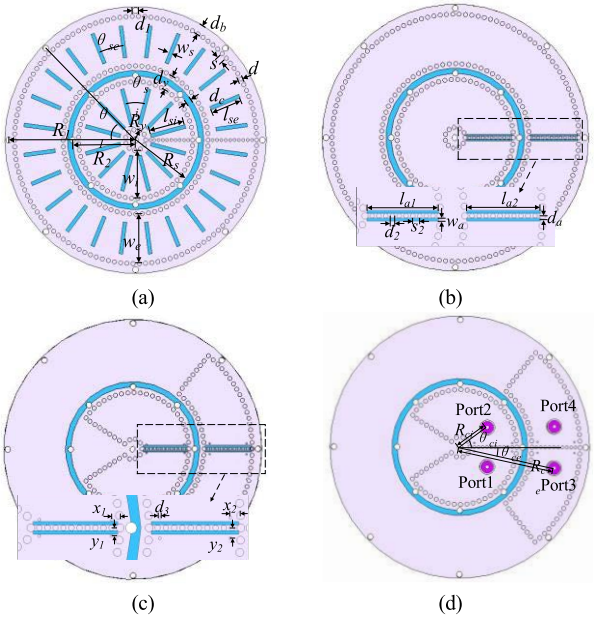

FIGURE 6. Configuration of the proposed array, (a) top view of the radiation layer, (b) back view of the radiation layer, (c) top view of the feeding layer, (d) back view of the feeding layer.

TABLE 1. Structural parameters of the proposed array.

s	s_2	d	d_c	d_1	d_b	d_v	d_2
2.1	1.4	1.4	1.8	2	3	5.2	1
d_a	d_3	θ_{si}	θ_{se}	θ_1	θ_{ci}	θ_{ce}	l_{si}
1.3	0.5	30°	15°	45°	35.5°	26.3°	12
l_{se}	l_{a1}	l_{a2}	w_i	w_e	w_s	w_a	R_1
10.5	15	15.5	15.8	16.3	1.2	0.6	42.6
R_2	R_v	R_{ci}	R_{ce}	x_1	x_2	y_1	y_2
21.2	3.4	11.3	32.5	1.5	1.9	1.4	1.8

of leaky wave antennas. In this paper, for ease of integration and fabrication, the LWA array is designed based on SIW.

Fig. 6 shows the structure of the double-layer LWA array. F4BM-2 substrate with $\varepsilon_r = 3.2$ and $\tan\delta = 0.002$ is chosen as the antenna dielectric. The thicknesses of radiation layer and feeding layer are set as $h_1 = 1$ mm and $h_2 = 3$ mm, respectively. In the feeding layer, four arc-shaped cavities and four ports are designed, among which port 1 and 3 are used as the feeding ports of radiating layer, and port 2 and 4 are terminated by 50 Ohm matched loads to absorb the rest power. In between the radiating and feeding layers, four coupled slots are notched for energy coupling. The radiating and feeding layers are compactly assembled by nylon screws. Finally, four co-axial probes are welded to the four ports. Structural parameters are listed in Table 1. The prototype of the array is shown in Fig. 7.

B. MEASUREMENT OF ANTENNA PERFORMANCE

It should be noted that for the proposed concentric LWA array, beam-changeable property is achieved by exciting the two LWAs individually and simultaneously. Thus, the designed array is tested under the two excitation types. Fig. 8 shows the $|S|$-parameters of the LWA array. It is observed that the isolations between the two LWAs are beyond 38 dB. The

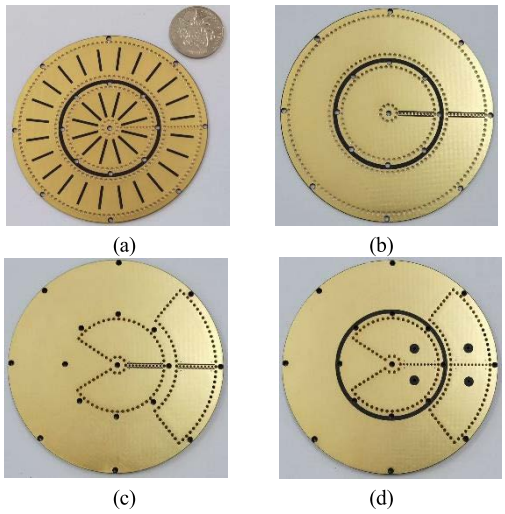

FIGURE 7. Prototype of the proposed array, (a) top view of the upper layer, (b) bottom view of the upper layer, (c) top view of the lower layer, (d) bottom view of the lower layer.

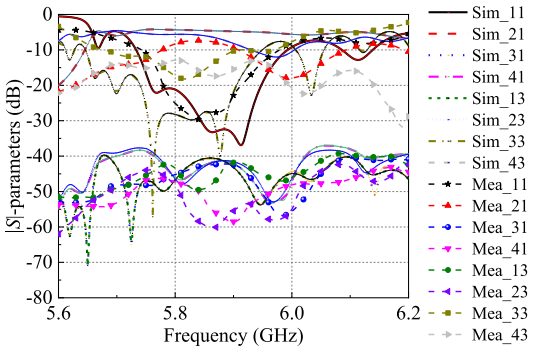

FIGURE 8. $|S|$-parameters of the proposed LWA array.

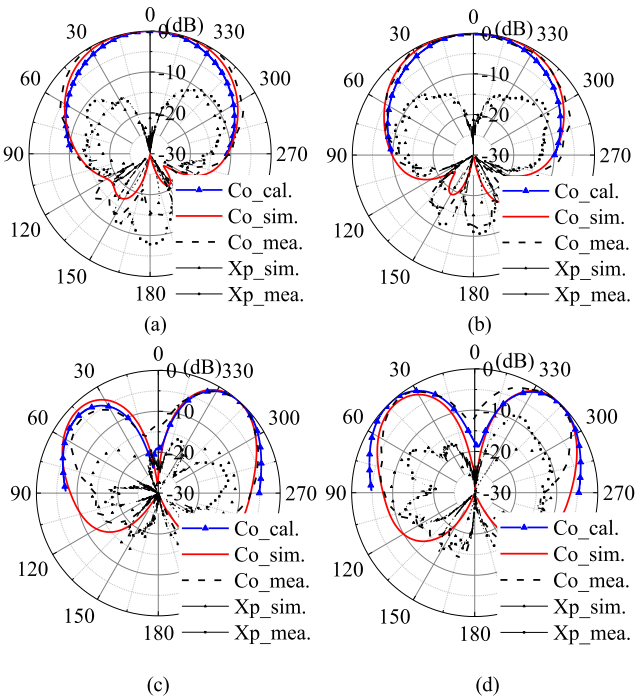

FIGURE 9. Radiation patterns of the LWA array when excited individually, (a) *xoz* -plane by exciting port 1, (b) *yoz* -plane by exciting port 1, (c) *xoz* -plane by exciting port 3, (d) *yoz* -plane by exciting port 3.

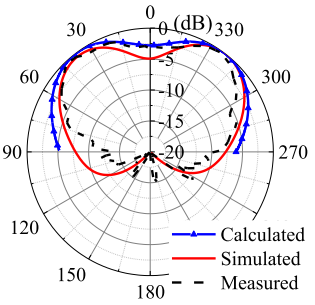

FIGURE 10. Radiation patterns of the LWA array in *yoz* -plane when exciting two elements in-phase simultaneously.

TABLE 2. Gains, axial ratios and efficiencies of the LWA array.

Ports	Sim. AR (dB)	Cal. AR (dB)	Mea. AR (dB)	Sim. Gain (dB)	Mea. Gain (dB)	Sim. Effi. (%)
1	1.5	0.55	0.62	2.19	1.59	44
3	2.48	2.89	1.59	1.28	3.49	41

difference between the measured and simulated results is mainly caused by the fabrication and welding tolerance.

Fig. 9 shows the radiation patterns of the array working under individual excitation. A broadside beam is generated by the inner LWA and a conical beam is generated by the outer LWA. The simulated, calculated and measured axial ratios and the simulated and measured gains and the simulated radiating efficiencies at 5.84 GHz are summarized in Table 2. The difference in gain is mainly due to the manufacture error and frequency shifting of the substrate which causes the changing of phase constant in the circular SIW and impacts the symmetry of the conical beam. The simulation efficiencies from the two ports are not very high, because higher radiating efficiencies for this structure will lead to undesired higher axial ratio. Because the corresponding parameters are $n_1 = 1$ and $n_2 = 3$, according to (5), there will be two main lobes when simultaneously exciting the two LWAs. Here, an in-phase bridge is applied to provide in-phase excitations for the two LWAs. As anticipated in the analysis in Section II-B, two main lobes are generated in *yoz*-plane as depicted in Fig. 10. Fig. 11 gives the axial ratio of the array when working under simultaneously excitation mode.

It can be observed that the measured results basically agree well with the results of full-wave simulation, and also agree with the calculated results of the proposed theoretical model. Furthermore, the beam angles of the array are listed in Table 2. The discrepancy of the measured and simulated results is mainly caused by the measurement error and fabrication tolerance. But the difference between the simulated and theoretical mode results are mainly caused by the assumption of infinite plane of the array aperture when using theoretical model.

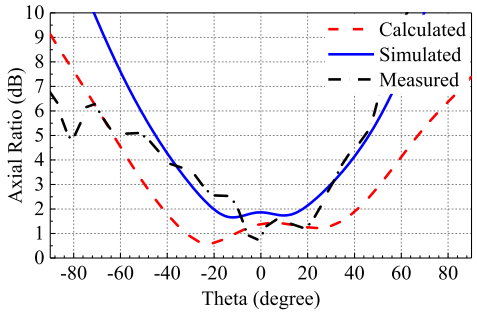

FIGURE 11. Axial Ratio in *yoz* -plane of the LWA array with simultaneously in-phase excitation.

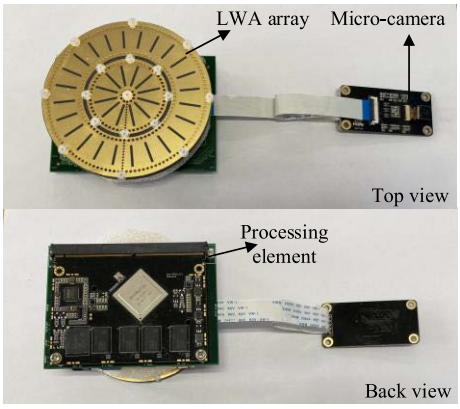

FIGURE 12. Prototype of the intellectualized antenna based on the double-loop array.

TABLE 3. Beam angles of the LWA array.

Ports	Plane	Sim. beam angle	Cal. beam angle	Mea. beam angle
1	*xoz*	2.7°	0°	5.3°
1	*yoz*	10.4°	1.0°	11.0°
3	*xoz*	40.1°	42°	39.5°
3	*yoz*	42.8°	44°	44.3°
1&3 (in phase)	*yoz*	37.0°	37.0°	36.0°

IV. APPLICATION TO SELF-SENSING SMART ANTENNA

In the previous work [17], a smart antenna integrated with image-aware function for automatic beam switching is proposed. Artificial-intelligence technology is used to determine the position of users. In this section, based on the proposed beam-changeable concentric annular LWA array of this paper and integrating the target detection method, a new self-sensing smart antenna for 2-D radio coverage, as illustrated in Fig. 12, is constructed. A series of tests are executed to see the performance of the self-sensing smart antenna.

A. SELF-SENSING AND BEAM-CHANGING

The principle diagram of the smart antenna is illustrated in Fig. 13. It is composed of a data acquisition element which uses one micro-camera, a data processing element (a micro-processor embedded with the target detection algorism), a single pole two throw switch, and a radiation element (the proposed antenna array). Here, the antenna array is working

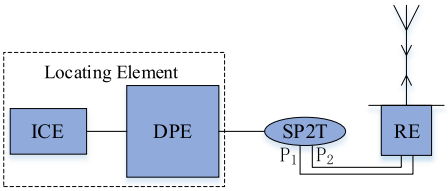

FIGURE 13. Principle diagram of the smart antenna. ICE, DPE, RE denote the image capturing element, data processing element and radiating element, respectively.

under multi-excitation mode. So, by feeding the two input ports of LWAs individually, the array provides two types of beams covering different regions. For acquiring the position of the user, all the detection information is extracted from the images of camera, and the two zone scores is given individually by [16]

$$Z^j = \frac{\sum_i C^{i,j} \times W_{Bbox}^{i,j} \times L_{Bbox}^{i,j}}{N \times W_{Zone} \times l_{Zone}} \tag{7}$$

where $C^{i,j}$ and $Bbox^{i,j}$ are configured by the deep neural network (DNN) integrated in the micro-processor, $C^{i,j}$ is the confidence rate of the corresponding *Bbox*, *Bbox* refers to the bounding box in the image to bound objects, i and j here denote the numbers of *Bboxes* and zones respectively, and N is the number of the boxes in one zone. Comparing with the other zone, the higher-scored one is seemed to be the optimized region for radio coverage.

The integrated DNN, Mobilenet [21], is a light-weighted target detection model with low latency, which is suitable to detect moving objectives. For the Mobilenet DNN, the micro-camera mainly aims to capture the images of the front view of people, while the DNN of this work is retrained to be adjusted for the top view of people. A series of recorded data is collected at several different places i.e. shopping malls, lecture buildings, etc. The training process is illustrated in Fig. 14. After pre-processing the data using Labeling to collect annotations of format VOC2007 [22], the processed data are loaded in batch at first, then an iterator is employed starting from shuffling, repeating, slicing and shuffling again to further train the parameters of the model. The effectiveness of the retraining is shown in Fig. 15. The retrained model is now capable of identifying a person from the top view. Thus, using equation (7), the positions of people are determined immediately and the beam is correspondingly changed to guarantee the wireless linking.

Fig. 16 presents the schematic diagram of the radiation scheme when a user moves within the monitored area. The data acquisition element keeps observing the monitored area like an eye captures images continuously. If there is no user inside the monitored area, the smart antenna will remain idle state with no radiation. Once a user emerges in zone 2, he will be detected by the camera and identified by DPE instantaneously, so that the position is determined by the locating element, and meanwhile, radiation will cover zone 2 by exciting port 3. As the user moves to zone 1, Port 1 will

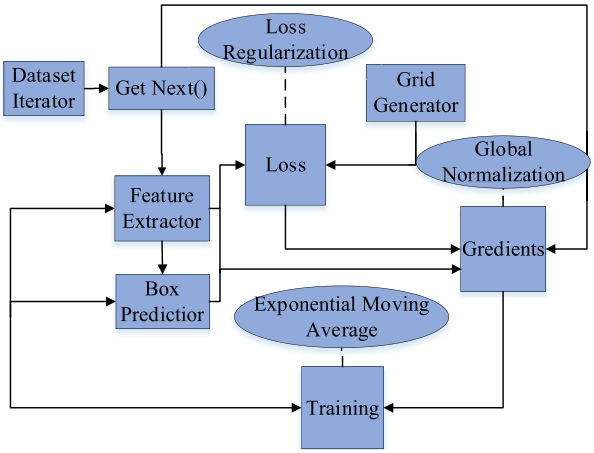

FIGURE 14. Model training procedure.

FIGURE 15. Illustration of the object detection of the modified model.

be excited by changing the excitation of SP2T and the main beam will change to zone 1 based on the same principle. In this way, the received power of the user is stabilized and the communication quality is guaranteed. It is noted that in order to adequately determine the trigger position for automatic excitation changing, the radiation characteristic of the antenna needs to be considered.

B. PERFORMANCE OF THE SELF-SENSING SMART ANTENNA

In order to verify the performance of the smart antenna, a series of measurements were carried out including received power distribution and Error Vector Magnitude (EVM) measurements in a real office scenario.

The size of the tested area is 4.2 m × 4.2 m. Fig. 17 shows the setup of the measurement system. The received power in the measured office is sampled by Agilent FieldFox RF Analyzer N9912A. The smart antenna (transmitting antenna) is mounted on an antenna holder with height of 2.67 m, and located at the center of the area. A signal generator of type R&S SMB100A is used to feed the antenna with power of 14 dBm at frequency of 5.84 GHz. The receiving antenna is an (RHCP) omnidirectional antenna and is fixed on an antenna platform with height of 0.7 m. During the test, the signal is received by the omnidirectional antenna and recorded by a PC connected to the analyzer, the spatial sampling interval is 60 mm.

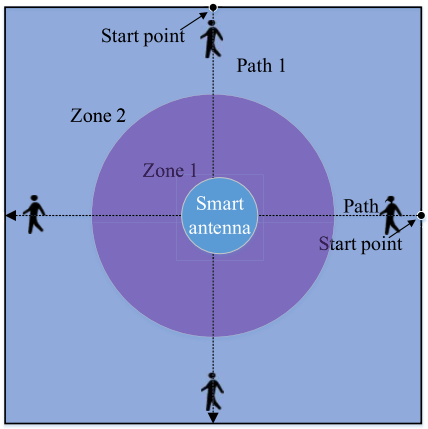

FIGURE 16. Operation diagram of the smart antenna.

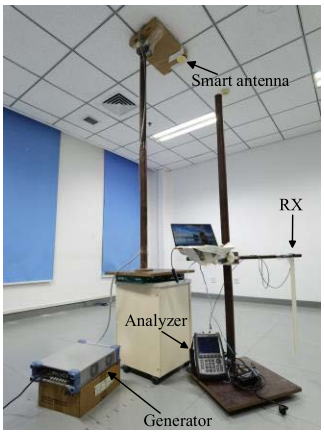

FIGURE 17. Set-up of received power test of the smart antenna.

TABLE 4. Average Value of EVM (%).

Operation mode	Path 1	Path 2
P_1_*only*	22.66	23.02
P_3_*only*	27.63	25.94
Smart	14.07	13.97

For verification and comparison, the radiation properties of the smart antenna are investigated first. Fig. 18 depicts the distributions of received power for the cases of exciting two array elements respectively. When Port 1 is excited, radio coverage occurs in zone 1, as shown by the contour in Fig. 18(a). When Port 3 is excited, radio coverage of zone 2 is provided, as illustrated in Fig. 18(b). When working in the smart mode, the beam of the antenna will automatically change according to a series of trigger positions, which are determined by a circle with a radius of 0.9 m in this paper, and the center of circle is just under the smart antenna. As seen in Fig. 19, when the antenna working on smart mode, more stable distributions of received power along path 1 and 2 can be acquired (from the angle of receiving), which are in between of -50 dBm and -40 dBm.

Furthermore, to investigate the performance of the smart antenna in a real wireless communication system, EVM is measured under the individual excitation mode and

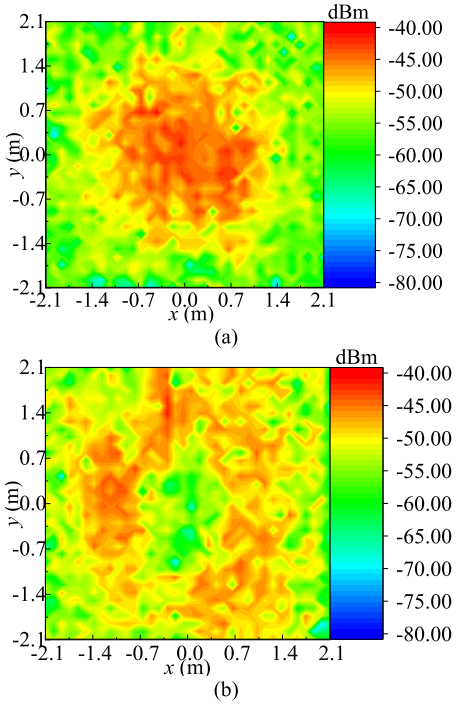

FIGURE 18. Distributions of measured received power for transmitting antenna operating in different excitation modes, (a) exciting port 1, (b) exciting port 3.

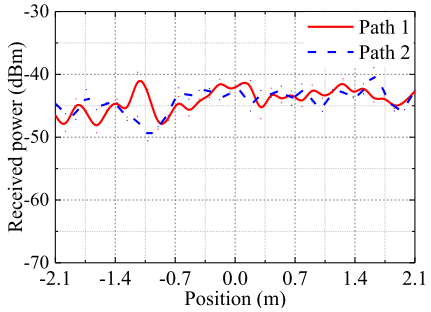

FIGURE 19. Distributions of measured received power for the smart antenna operating in automatic beam-changing mode along Path 1 and Path 2.

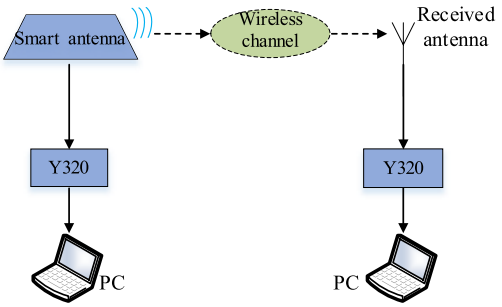

FIGURE 20. Lock diagram of EVM test's set-up.

smart mode respectively along the two paths in Fig 16. Schematic diagram of the communication system is shown in Fig. 20. A pair of YunSDR Y320 baseband modules is employed, comprising of a generator, encoder and decoder etc. Quadrature phase shift keying (QPSK) modulation mode is applied during the measurement. The data frames with a

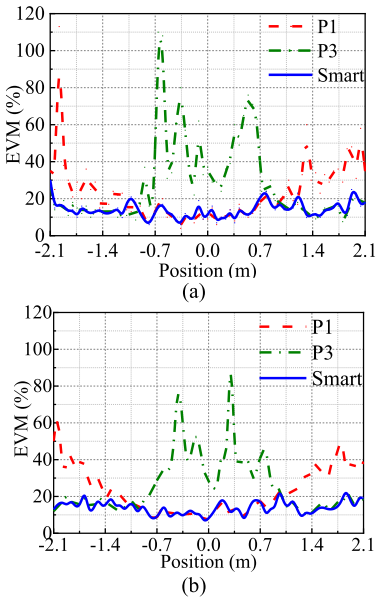

FIGURE 21. Distributions of EVM for transmitting antenna operating in different modes along (a) Path 1 and (b) Path 2. The dashed and dashed-dot lines correspond to the measured results for individual excitations (without beam-changing), the results in solid line are measured when the smart antenna is operated in smart mode in terms of position information of users.

bandwidth of 20 Mbps are modulated on a carrier frequency of 5.84 GHz. When the two ports are excited individually, as the dashed and dashed-dot lines in Fig. 21(a) and (b) show, EVM is lower in zone 1 and 2 but is very high in the rest of the area. In these cases, users will experience bad communication quality in the region with poor radiation. As the solid curves depict, it is distinctly seen that the smart mode of antenna leads to lower and more stable EVM, most of which are below 22 % along both paths. More exactly, the average EVM in different modes along path 1 and 2 are presented in table 3. Average EVM of the case of automatic beam-changing (14.07% along path 1 and 14.97% along path 2) is significantly smaller than those of individual excitation of the antenna. Therefore, the smart antenna has the merit of improving the communication quality in a wireless communication system.

V. CONCLUSION

In this paper, a concentric LWA array is designed, which is capable of changing its beam between different shapes and orientations. For analyzing the radiating characteristics, a theoretical model is established, by which a prototype is designed and fabricated. The measurement results verify the correction of calculation results of the theoretical model and simulation results of the full-wave simulation, and show an expected performance. Furthermore, based on the proposed antenna, a self-sensing and automatic beam changing smart antenna based on image-aware circuit is constructed. The smart antenna is tested in a real office scenario, and good performance is observed through the received power and EVM measurement results. Therefore, the proposed

smart antenna is a promising candidate for smart wireless communication applications.

REFERENCES

[1] F. Y. Xia, Y. J. Cheng, Y. F. Wu, and Y. Fan, "V-band wideband circularly polarized endfire multibeam antenna with wide beam coverage," *IEEE Antennas Wireless Propag. Lett.*, vol. 18, no. 8, pp. 1616–1620, Aug. 2019.

[2] J.-W. Lian, Y.-L. Ban, H. Zhu, and Y. J. Guo, "Reduced-sidelobe multibeam array antenna based on SIW Rotman lens," *IEEE Antennas Wireless Propag. Lett.*, vol. 19, no. 1, pp. 188–192, Jan. 2020.

[3] X. Wang, X. Fang, M. Laabs, and D. Plettemeier, "Compact 2-D multibeam array antenna fed by planar cascaded Butler matrix for millimeter-wave communication," *IEEE Antennas Wireless Propag. Lett.*, vol. 18, no. 10, pp. 2056–2060, Oct. 2019.

[4] M. Movahhedi, M. Karimipour, and N. Komjani, "Multibeam bidirectional wideband/wide-scanning-angle holographic leaky-wave antenna," *IEEE Antennas Wireless Propag. Lett.*, vol. 18, no. 7, pp. 1507–1511, Jul. 2019.

[5] Y. Bi, Y. Li, and J. Wang, "3-D printed wideband Cassegrain antenna with a concave subreflector for 5G millimeter-wave 2-D multibeam applications," *IEEE Trans. Antennas Propag.*, vol. 68, no. 6, pp. 4362–4371, Jun. 2020.

[6] J.-W. Lian, H. Zhu, Y.-L. Ban, D. K. Karmokar, and Y. J. Guo, "Uniplanar high-gain 2-D scanning leaky-wave multibeam array antenna at fixed frequency," *IEEE Trans. Antennas Propag.*, vol. 68, no. 7, pp. 5257–5268, Jul. 2020.

[7] Z. H. Jiang, Y. Zhang, J. Xu, Y. Yu, and W. Hong, "Integrated broadband circularly polarized multibeam antennas using berry-phase transmit-arrays for *Ka*-band applications," *IEEE Trans. Antennas Propag.*, vol. 68, no. 2, pp. 859–872, Feb. 2020.

[8] C. Song, E. L. Bennett, J. Xiao, T. Jia, R. Pei, K.-M. Luk, and Y. Huang, "Passive beam-steering gravitational liquid antennas," *IEEE Trans. Antennas Propag.*, vol. 68, no. 4, pp. 3207–3212, Apr. 2020.

[9] D. Hua, S.-S. Qi, W. Wu, and D.-G. Fang, "Synthesis of conical beam array antenna with concentric loop configuration using element-level pattern diversity technique," *IEEE Trans. Antennas Propag.*, vol. 66, no. 11, pp. 6397–6402, Nov. 2018.

[10] H. Li, S. Sun, W. Li, M. Wu, and C. Zhou, "Systematic pattern synthesis for single antennas using characteristic mode analysis," *IEEE Trans. Antennas Propag.*, vol. 68, no. 7, pp. 5199–5208, Jul. 2020.

[11] S. Ahdi Rezaeieh, A. Zamani, and A. M. Abbosh, "Pattern reconfigurable wideband loop antenna for thorax imaging," *IEEE Trans. Antennas Propag.*, vol. 67, no. 8, pp. 5104–5114, Aug. 2019.

[12] X. Yang, Y. Liu, H. Lei, Y. Jia, P. Zhu, and Z. Zhou, "A radiation pattern reconfigurable Fabry–Pérot antenna based on liquid metal," *IEEE Trans. Antennas Propag.*, vol. 68, no. 11, pp. 7658–7663, Nov. 2020.

[13] J. Wang, W.-B. Lu, Z.-G. Liu, A.-Q. Zhang, and H. Chen, "Graphene-based microwave antennas with reconfigurable pattern," *IEEE Trans. Antennas Propag.*, vol. 68, no. 4, pp. 2504–2510, Apr. 2020.

[14] X. G. Zhang, W. X. Jiang, H. W. Tian, Z. X. Wang, Q. Wang, and T. J. Cui, "Pattern-reconfigurable planar array antenna characterized by digital coding method," *IEEE Trans. Antennas Propag.*, vol. 68, no. 2, pp. 1170–1175, Feb. 2020.

[15] B. Ahn, H.-W. Jo, J.-S. Yoo, J.-W. Yu, and H. L. Lee, "Pattern reconfigurable high gain spherical dielectric resonator antenna operating on higher order mode," *IEEE Antennas Wireless Propag. Lett.*, vol. 18, no. 1, pp. 128–132, Jan. 2019.

[16] Y. Ma, J. Wang, Y. Li, M. Chen, Z. Li, and Z. Zhang, "Smart antenna with automatic beam switching for mobile communication," *EURASIP J. Wireless Commun. Netw.*, vol. 2020, no. 1, p. 179, Dec. 2020.

[17] Y. Ma, W. Tian, J. Wang, W. Hou, Y. Li, M. Chen, Z. Li, and Z. Zhang, "An image-aware based smart antenna capable of automatic beam switching for indoor mobile communication," *IEEE Access*, vol. 8, pp. 379–388, 2020.

[18] Y. Ma, J. Wang, Z. Li, Y. Li, M. Chen, and Z. Zhang, "Planar annular leaky-wave antenna array with conical beam," *IEEE Trans. Antennas Propag.*, vol. 68, no. 7, pp. 5405–5414, Jul. 2020.

[19] F. Xu and K. Wu, "Guided-wave and leakage characteristics of substrate integrated waveguide," *IEEE Trans. Microw. Theory Techn.*, vol. 53, no. 1, pp. 66–73, Jan. 2005.

[20] Y. Geng, J. Wang, Y. Li, Z. Li, M. Chen, and Z. Zhang, "New design of beam-formed leaky-wave antenna based on substrate integrated waveguide in a confined space," *IEEE Trans. Antennas Propag.*, vol. 66, no. 11, pp. 6334–6339, Nov. 2018.

[21] A. G. Howard, M. Zhu, B. Chen, D. Kalenichenko, W. Wang, T. Weyand, M. Andreetto, and H. Adam, "MobileNets: Efficient convolutional neural networks for mobile vision applications," 2017, *arXiv:1704.04861*.

[22] M. Everingham, L. Van Gool, C. K. I. Williams, J. Winn, and A. Zisserman. (2007). *The PASCAL Visual Object Classes Challenge 2007 (VOC2007) Results*. [Online]. Available: http://www.pascal-network.org/challenges/VOC/voc2007/workshop/index.html

YUCHEN MA was born in Beijing, China, in 1993. He received the B.E. and Ph.D. degrees from the School of Electronic and Information Engineering, Beijing Jiaotong University, Beijing, in 2015 and 2021, respectively. He is currently with the China Academy of Information and Communications Technology, Beijing. His current research interests include near-field measurement and antenna design.

JUNHONG WANG (Senior Member, IEEE) was born in Jiangsu, China, in 1965. He received the B.S. and M.S. degrees in electrical engineering from the University of Electronic Science and Technology of China, Chengdu, China, in 1988 and 1991, respectively, and the Ph.D. degree in electrical engineering from Southwest Jiaotong University, Chengdu, in 1994. In 1995, he joined the Department of Electrical Engineering, Beijing Jiaotong University, Beijing, China, as a Faculty, where he became a Professor, in 1999. From January 1999 to June 2000, he was a Research Associate with the Department of Electric Engineering, City University of Hong Kong, Hong Kong. From July 2002 to July 2003, he was a Research Scientist with Temasek Laboratories, National University of Singapore, Singapore. He is currently with the Key Laboratory of all Optical Network and Advanced Telecommunication Network, Ministry of Education of China, Beijing Jiaotong University, and also with the Institute of Lightwave Technology, Beijing Jiaotong University. His research interests include numerical methods, antennas, scattering, and leaky wave structures.

CHONG PAN was born in Harbin, China, in 1982. He received the master's degree from the Beijing University of Posts and Telecommunications. He is currently working at the China Academy of Information and Communications Technology, Beijing, China. His current research interest includes RF OTA testing.

YING ZHU was born in Shanxi, China, in 1987. She received the M.Sc. degree in wireless communications and signal processing from the University of Bristol, in 2012. She is currently a Senior Engineer with the China Academy of Information and Communications Technology. Her current research interests include 5G standardization and advanced testing methodologies.

XIANG WU was born in Beijing, China, in 1979. He received the M.E. and M.Sc. degrees from the School of Electronic and Information Engineering, Beijing Jiaotong University, Beijing, China, in 2002 and 2005, respectively. He is currently with the China Academy of Information and Communications Technology, Beijing. His current research interests include ICV, OTA, and antenna design.